RESEARCH PAPER

Pulsed Laser Deposition (PLD) to Synthesis of $NiZnFe_2O_4$ Nanoparticles

Wala Gazey Mahmood Dizayee

Department of General Sciences, College of Basic Education, Salahaddin University-Erbil, Erbil, Kurdistan Region, Iraq

ARTICLE INFO

Article History:
Received 11 March 2023
Accepted 21 May 2023
Published 01 July 2023

Keywords:
Nanoparticles
Nickel ferrite
Pulsed laser deposition
Thin film
Zinc ferrite

ABSTRACT

In this study, crystalline nanoparticles of ferrite compound with the formula of $Ni_{0.5}Zn_{0.5}Fe_2O_4$ have been synthesized and deposited on the Si substrate by a physical method known as Pulsed Laser Deposition (PLD) method. The physicochemical properties and microstructure of the resultant Zn/Ni ferrite-deposited thin films were investigated using different characterization techniques including XRD, SEM, AFM and FTIR techniques. Uniform and evenly distributed nanoparticles on the Si surface were observed in SEM and AFM analysis. Moreover, the morphological studies revealed that the deposited-nanoparticles grains are clear with well-defined grain boundaries. Some droplet and cluster aggregates were also observed in morphological analysis, which are related to the sample ablation during PLD process due to incomplete elimination of target splashing. The FTIR spectra showed the characteristic chemical bands of the materials used for the fabrication of nanoparticles and thin films. The single-phase cubic spinel structure of samples has been confirmed from X-ray diffraction analysis.

How to cite this article
Mahmood DizayeeM. G. Pulsed Laser Deposition (PLD) to Synthesis of $NiZnFe_2O_4$ Nanoparticles. J Nanostruct, 2023; 13(3):863-870. DOI: 10.22052/JNS.2023.03.027

INTRODUCTION

Recently, one-dimensional (1D) nanostructures have attracted a great deal of interest due to their unique electronic, magnetic and physical properties[1]. Among various nanoscale materials, spinel ferrites (MFe_2O_4; M = Fe, Co, Ni, Mn, Zn, etc.) have become attractive due to their wide practical applications in different fields of the science and technology such as magnetic refrigeration, ferrofluids making, magnetic resonance imaging and high-density data storage[2-5]. These nanoscale structures also found potential applications in other areas such as biomedical, wastewater treatment, catalyst and electronic device with or without other additives [6-9]. Among these materials, nickel ferrite ($NiFe_2O_4$) is one of the most important spinel ferrites, and it is especially attractive to researchers because of its high magneto crystalline anisotropy, high saturation magnetization and unique magnetic structure[10]. These structures exhibit various kinds of magnetic properties, including paramagnetic, superparamagnetic or ferrimagnetic behavior, by varying their particle size and shape[11, 12].

The unit cell regarding spinel ferrites comprises 32 oxygen atoms packed closely together in cubic positions, with 16 occupied octahedral sites and eight tetrahedral voids. In a typical spinel, all 16 trivalent elements and 8 divalent elements are organized in octahedral spaces. While the 2-valent elements are also organized in inverse spinel's

* *Corresponding Author Email: wala.dizayee@su.edu.krd*

octahedral spaces, the three-valent elements are split evenly between tetrahedral spaces and cathedral spaces (Fig. 1) [13-15].

The distribution of the cations can impact the mutation of the electrons, interactions of the magnetic exchange, and modification of magnetic characteristics, and therefore, expand and enhance the ferrite applications[16-18]. Using these materials is wide-ranging as a result of the abovementioned modifications, as well as the fact that they can reach a variety of qualities like the coercive force, magnetic permeability, saturation magnetization (μS), anisotropy constant, physical and chemical stability, and mechanical stiffness. As a result, neuromas studies have been conducted on the production and modification of the magnetic characteristics of ferrites as well as doping effects of various 2/3-valent elements within their structures[18-21]. Cobalt ferrite is one of these structures due to its good saturation magnetization (MS), high coercive force (HC), high magnetic permeability, mechanical hardness, and excellent chemical and physical stability. As a result, it is a perfect choice for radar absorption materials (RAM), Ferro-fluid technology, drug delivery, high-density magnetic recording, magnetic hyperthermia (MH) for cancerous tissues, and magnetic resonance imaging (MRI)[8, 22-24].

Inverse spinel structure is present in cobalt ferrite ($CoFe_2O_4$). Accordingly, half of the 3-valent iron ions are in tetrahedral spaces, while the second half is in octahedral sites for 2-valent cobalt ions, which are in octahedral locations. However, zinc is a cheap substance and may considered for doping into the cobalt ferrite in order to produce appropriate magnetic characteristics, in particular, for the applications involving hyperthermia[25, 26]. In these structures, as a typical spinel, zinc ferrite contains all of the 3-valent ions in octahedral regions and 2-valent ions in tetrahedral places. This could explain why Zn-doped cobalt ferrite structures may have modified spinel structure $(Zn^{2+}_{x}Fe^{3+}_{1-x})_A\ [Co^{2+}_{1-x}Fe^{3+}_{1+x}]_BO_4$ [14, 24, 27, 28].

The production of zinc cobalt ferrite is of tremendous interest because of its potential applications in a range of domains. The size, shape, and other physicochemical properties of synthetic ferrites affect their final applications[29]. There are several methods to prepare magnetic nanoparticles (gaseous, solid, and liquid phase synthesis)[30-32]. Pulsed Laser Deposition (PLD) is a thin-film deposition technique that is used frequently for in stiu synthesizing and deposition of different nanoscale materials. This method uses high-energy laser pulses to vaporize the surface of a solid target inside a vacuum chamber and condense it on a substrate to form nanoparticles or thin films up to a few micrometers in thickness[33, 34].

In this study, the PLD technique has been used to synthesize ferrite compounds with the formula of $Ni_{0.5}Zn_{0.5}Fe_2O_4$. The physicochemical, morphological and crystalline properties of the resultant nano Zn-ferrite were investigated by different characterization methods including SEM, AFM, XRD, and FTIR techniques.

MATERIALS AND METHODS

Materials and reagents

Iron nitrate [$(Fe(NO_3)_3.9H_2O)$], nickel nitrate [$(Ni(NO_3)_2.6H_2O)$], Zinc nitrate [$Zn(NO_3)_2.6H_2O$]

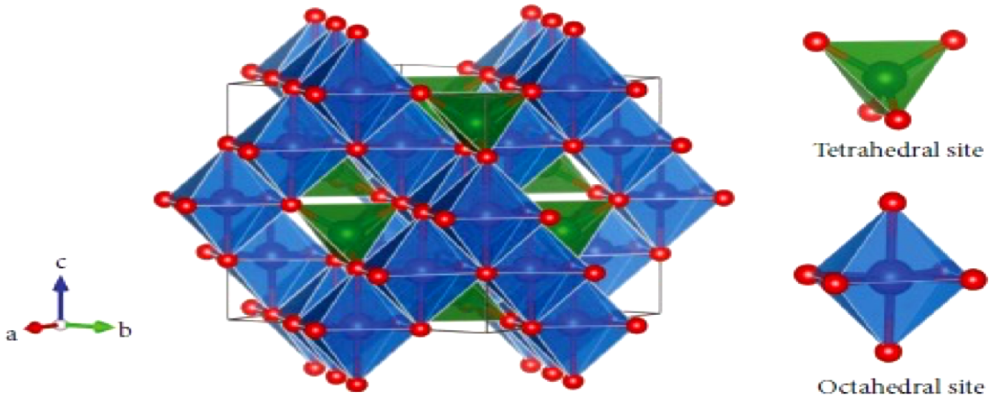

Fig. 1. Cubic spinel structure. Electron (-e) locations of the oxygen have been depicted in red, whereas octahedral and tetrahedral cation sites have been represented in blue and green, respectively.

and citric acid (99%) were purchased from Sigma–Aldrich chemical reagent Co. (USA). All the reagents were of analytical grade with a high purity of 99.99% and used as received without further purification.

Preparation of $NiZnFe_2O_4$ Nanoparticles by PLD

The nitrate compounds of nickel, zinc and iron with a molar ratio of (0.5:0.5:2) were combined with citric acid (1:2) as the host to create nano-powder of cations. The powder that was thus produced was hydraulically pressed into pellet shape. The pellet was sintered for three hours at 1200°C. The substrate used for film deposition was Si (100) of size 10 × 10 mm. A Lambda Physik KrF excimer laser (model COMPex 102 and PLD chamber) of wavelength 248 nm has been used to deposit Ni/Zn ferrite films on Si substrate. Pulse energy was adjusted to 220 mJ, pulse duration 20 ns, and repetition rate was kept 10 Hz. The laser beam was directed at 45° from the target normal and focused on a 3.5 × 0.5 mm^2 area of the ablated target. The deposition of the thin films was done in a high-vacuum chamber, which was evacuated to a base pressure lower of 1×10^{-6} Torr by means of a SD-200 Turbo V200 pump. The gas pressure inside the PLD chamber was measured using a cold cathode gauge and adjusted via an electronic mass flow controller. The substrate was mounted at a distance of 4 cm from the target. The substrate temperature was kept 600 °C. Flowing O_2 gas pressure at 100 mTorr was used during deposition process in order to preserve the stoichiometry in the films. The deposition was carried out under constant laser energy to reduce the occurrence of ferrite droplets caused by splashing from the target. Fig. 2, Schematically represent the sample preparation and PLD process used in this study for deposition of nanoparticles on Si substrate.

Characterization

The morphological characteristic of the nanoparticles-deposited thin films was studied by SEM analysis using Scanning Electron Microscopy (Philips XL 30 and VEGA\\TESCAN) instrument at 30 kV. The particle size distribution of the prepared nanoparticles-deposited thin films was analyzed by determining the size of about 100 randomly

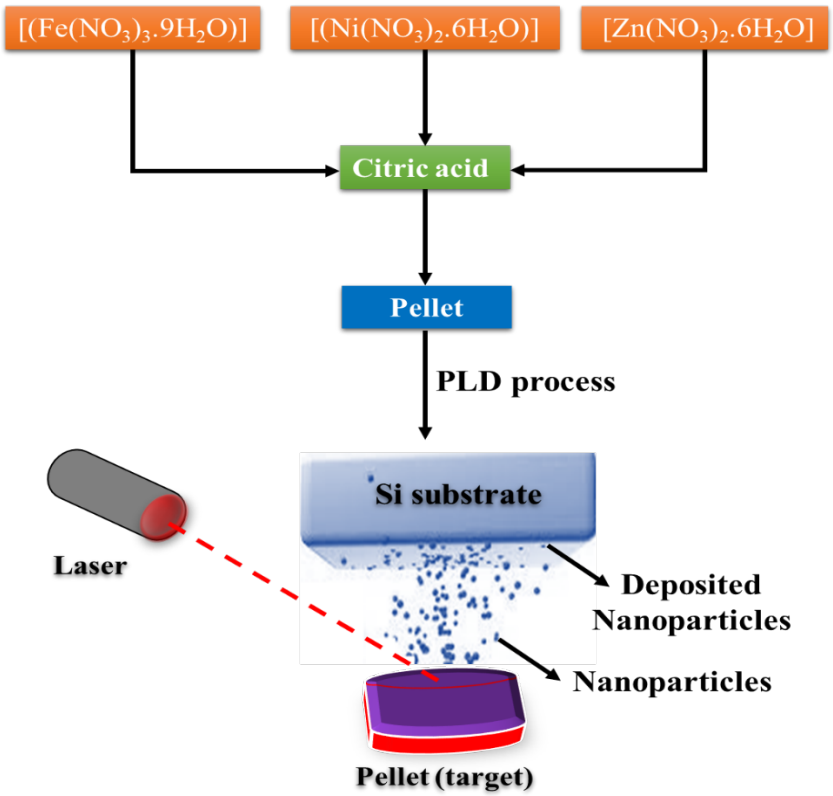

Fig. 2. Schematic illustration of sample preparation and PLD process for deposition of nanoparticles on Si substrate.

selected particles using ImageJ 1.52v software (National Institutes of Health, USA, http://imagej.nih.gov/ij/). To examine the surface morphology and topography of the samples, atomic force microscopy (AFM) was applied using a silicon nitride cantilever in contact mode on the Nano scope E Digital equipment. The cantilever's force constant was 0.56 N/m, and the tip radius was 20 nm. The chemical structure and composition of the resultant thin films were investigated using an FTIR instrument (FTIR, Bruker Model Vertex 70 FTIR, Germany) in the range 500-1000 cm^{-1}. The crystalline structure of films was examined by X-ray diffraction method using the SCINTAG DMS 2000 XRD equipment in a θ-2θ configuration with Cu-K radiation (λ = 1.93604 Å).

RESULTS AND DISCUSSION

SEM and AFM analysis

Fig. 3 shows the SEM images of the nanoparticle deposited on Si thin films. As we can see from the background of Fig. 3A, the prepared thin films exhibited a smooth blacked surface with several droplet contamination in the nanoscale sizes, which is often associated with PLD[31, 35]. The occurrence of these droplets is the result of incomplete elimination of target splashing during laser ablation, in spite of the lower energies of the laser beam. The high repetition rate of the laser pulses, which is required to ensure a high deposition rate, may cause droplets and cluster aggregates to occur during ablation. The repetition and deposition rate of 5 Hz and 2 nm/min were considered an optimum values for growing good quality Ni/Zn ferrite on thin films[36]. In order to further investigate the surface morphology features of the prepared Ni/Zn ferrite thin films, the size distribution of the droplet contamination was measured by ImageJ software and the results are depicted in Fig. 4. As we can see, the size distribution of the droplet contamination is in the nanoscale size with an average size of 147.40 ± 119.25 nm. These results confirm the successful synthesizing and deposition of Ni/Zn ferrite nanoparticles on Si thin films. Moreover, regarding the nanoscale size of these droplets, we can conclude that the majority of the nanoparticles were less than these sizes, resulting in highly uniform and smooth-surfaced thin films.

The AFM images of the prepared thin films in Fig. 5 also depicted typical thin film surfaces with visibly displaying smooth surfaces and good optical quality and definition. In agreement with SEM images, the deposited nanoparticles on the surface of thin films, along with droplet contamination from target splashing, resulted in a grainy appearance of the resultant thin film surfaces. However, as we can see, all AFM images from the prepared thin film surfaces represented a highly smooth and uniform deposition of nanoparticles. This resulted in considerably even surface topography for resultant thin films, which is a desired feature for obtaining unique and specific properties from these samples.

FT-IR analysis

The typical spectra of the FT-IR regarding the prepared Ni/Zn ferrite nanoparticle-deposited

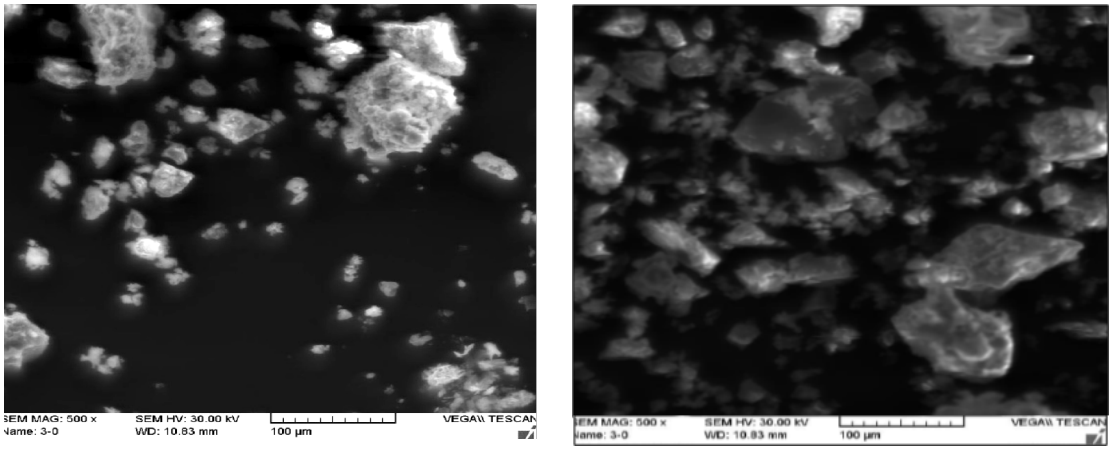

Fig. 3. The SEM images of the prepared Ni/Zn ferrite-deposited thin films captured from different positions (A and B) of the thin films.

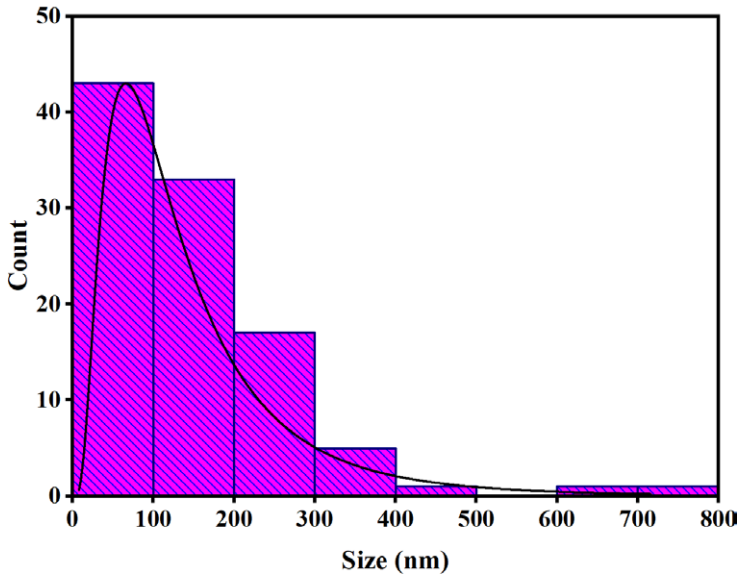

Fig. 4. The size distribution of the droplet contamination occurred during PLD process.

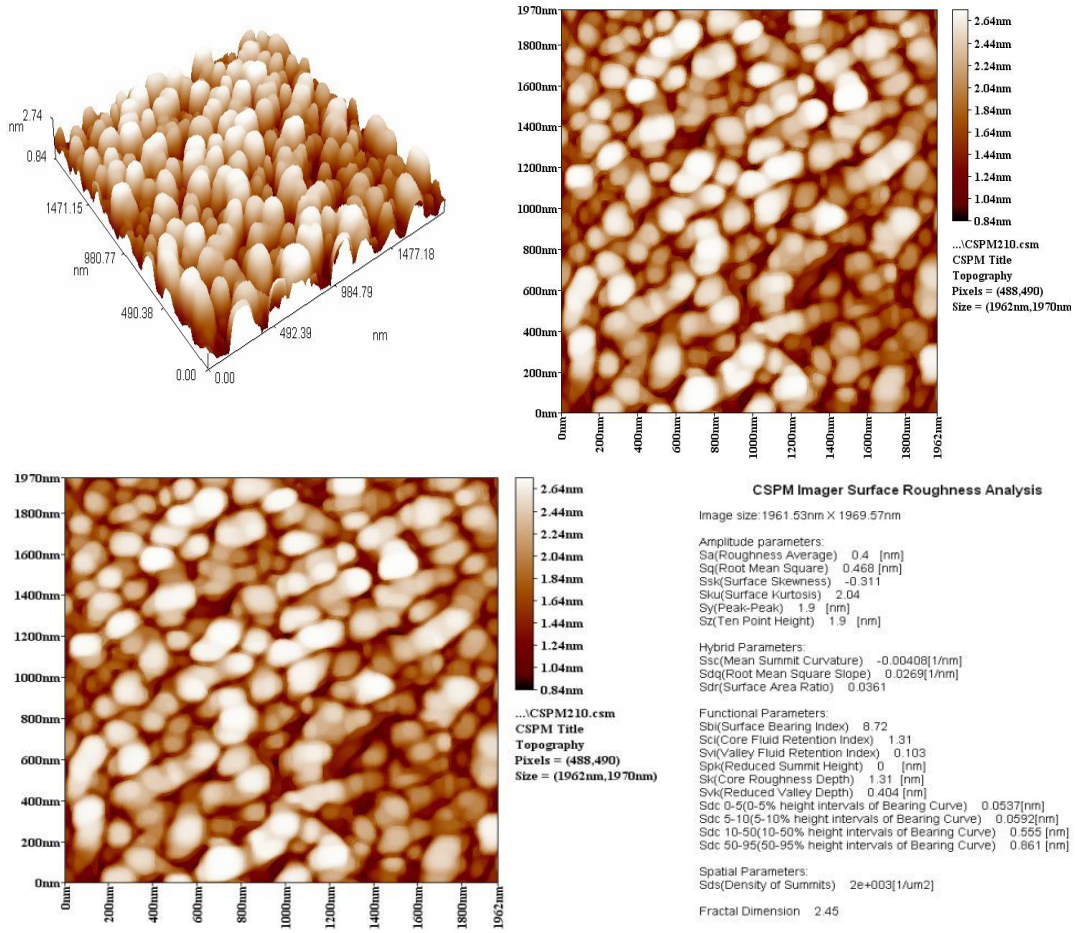

Fig. 5. AFM images of the prepared Ni/Zn ferrite-deposited thin films captured from different positions of the thin films.

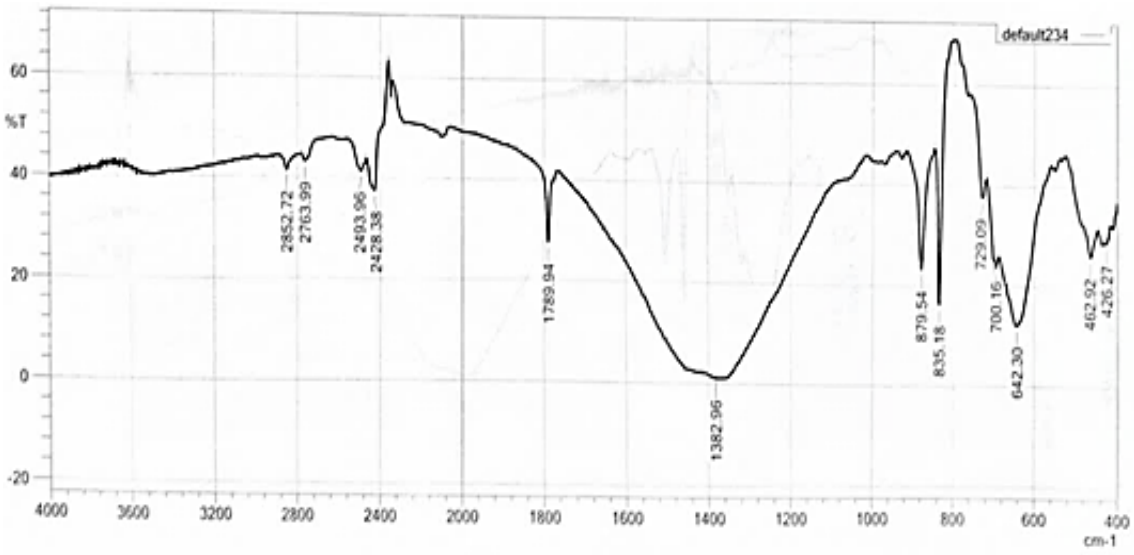

Fig. 6. FT-IR spectra of the prepared Ni/Zn ferrite-deposited thin films.

thin films have been depicted in Fig. 6. FT-IR spectra were used for identifying the ferrite phase's development. The peaks observed at 426.27 cm^{-1} and 462.92 cm^{-1} are the peaks of the metal-oxygen vibration extended towards the tetrahedral and octahedral site (at sites A and B, discussed above) with a pure cubic spinel ferrite structure, which confirms the formation of Ni/Zn-doped ferrite nanoparticles. The comparatively lower wavenumbers (which are generally detected at 544–569 cm^{-1}) are due to the octahedral metal–oxygen vibrational band at 400–500 cm^{-1}. At 426.27 cm^{-1}, the lower wavenumber absorption band was extra sharp for the octahedral sites,

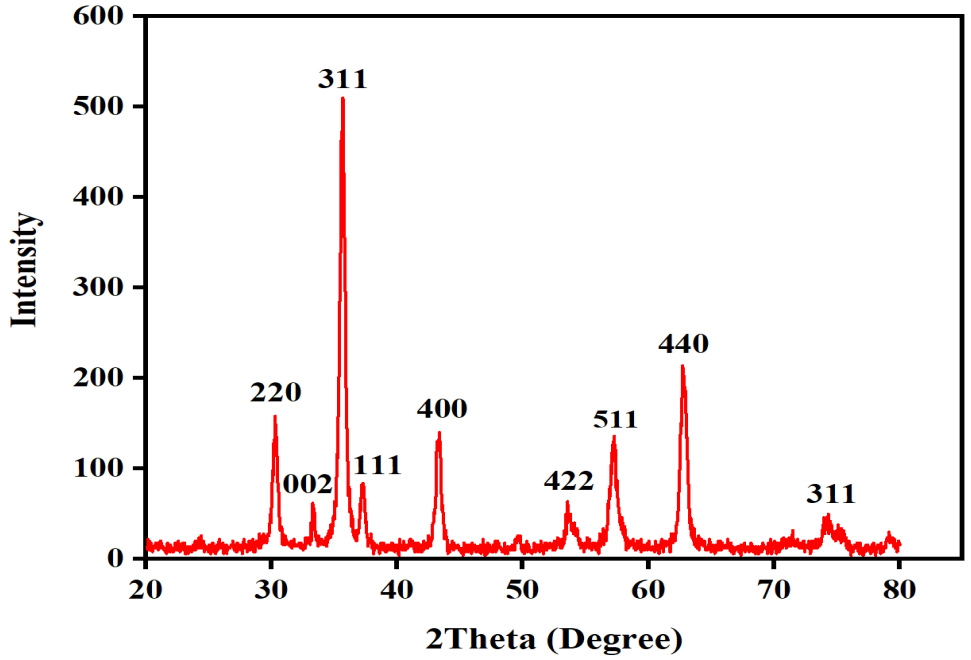

Fig. 7. XRD pattern of the prepared Ni/Zn ferrite-deposited thin films.

while the band at 462.92 cm^{-1} signifies the tetrahedral sites in the inverse spinel structure of $Ni_{0.5}Zn_{0.5}Fe_2O_4$[7, 37]. The broad peak at 3400 cm^{-1} is due to the chemisorbed water molecule and having an HO-H bond[38]. The remaining peaks could be attributed to the Si (100) and citric acid vibrations used as a substrate or host material for the fabrication and deposition of nanoparticles. In this regard, the 1789.94 cm^{-1} peak was attributed to carbonyl groups of the citric acid, while the two peaks at 2852.72 cm^{-1} and 2763.99 cm^{-1} were attributed to its asymmetric and symmetric -CH_2 groups vibration stretching. The broad peak at 1382.96 is also related to the vibration of C-O bonds of citric acid[39, 40].

X-ray Diffractometer (XRD)

Fig. 7 illustrates XRD patterns of synthesized $Ni_{0.5}Zn_{0.5}Fe_2O_4$-deposited thin film nanocomposites. From this figure, all the observed diffraction peaks can be indexed to a cubic spinel phase (in agreement with the FTIR spectra section) with FCC structure magnetite according to JCPDS card No 82-1042. Nine characteristic XRD peaks marked by their Miller indices (220), (002), (311), (111), (400), (422), (511), (440) and (311) at 2θ values of 30.28°, 33.28°, 35.68°, 37.28°, 43.36°, 53.56°, 57.28°, 62.76°, and 74.32°. All of the XRD peaks were matched with JCPDS cards 8–1935 ($MgFe_2O_4$) and 89-1012 ($ZnFe_2O_4$)[37, 41]. Moreover, the (002), (111) and (311) peaks at 33.28, 37.28, and 74.32 were attributed to the Ni_2O_3, Ni and NiO crystalline structure the resultant thin films[41, 42]. The most intense peak detected for the (311) plane clearly proves the formation of the cubic spinel ferrite structure, with other major diffraction planes being observed at different 2θ angles.

CONCLUSION

Pulsed laser deposition has been successfully used as the target to create $Ni_{0.5}Zn_{0.5}Fe_2O_4$ nanoparticles with an optimal structure on the Si substrate thin films.

A uniform and evenly distributed nanoparticles on the Si surface were observed in SEM and AFM analysis. The morphological studies also revealed that the grains are clear with well-defined grain boundaries. Moreover, some droplet and cluster aggregates also observed in SEM and AFM images, which is occurred due to the incomplete elimination of target splashing during ablation. The FTIR spectra showed the characteristic chemical bands of the materials used for the fabrication of thin films. The single-phase cubic spinel structure of samples has been confirmed from X-ray diffraction analysis. Furthermore, it was noted that the PLD-synthesized and deposited nanoparticles had extremely small and nanoscale particle sizes. Therefore, it can be concluded that PLD is a superior synthesizing and nanoparticle deposition method for producing desired nanoparticle-deposited thin films.

CONFLICT OF INTEREST

The authors declare that there is no conflict of interests regarding the publication of this manuscript.

REFERENCES

1. Xia Y, Yang P, Sun Y, Wu Y, Mayers B, Gates B, et al. One-Dimensional Nanostructures: Synthesis, Characterization, and Applications. Adv Mater. 2003;15(5):353-389.
2. Sivakumar P, Ramesh R, Ramanand A, Ponnusamy S, Muthamizhchelvan C. Synthesis and characterization of $NiFe_2O_4$ nanoparticles and nanorods. Journal of Alloys and Compounds. 2013;563:6-11.
3. Raj K, Moskowitz B, Casciari R. Advances in ferrofluid technology. Journal of Magnetism and Magnetic Materials. 1995;149(1-2):174-180.
4. Abazari M, Ghaffari A, Rashidzadeh H, Momeni badeleh S, Maleki Y. Current status and future outlook of nano-based systems for burn wound management. Journal of Biomedical Materials Research Part B: Applied Biomaterials. 2019;108(5):1934-1952.
5. Rashidzadeh H, Mozafari F, Ghaffarlou M, Barsbay M, Ramazani A, Abazari M, et al. Harnessing the Power of Nanomaterials to Alleviate Tumor Hypoxia in Favor of Cancer Therapy. Harnessing Materials for X-ray Based Cancer Therapy and Imaging: Springer International Publishing; 2022. p. 135-174.
6. Akbarzadeh A, Samiei M, Davaran S. Magnetic nanoparticles: preparation, physical properties, and applications in biomedicine. Nanoscale Research Letters. 2012;7(1).
7. Kefeni KK, Msagati TAM, Mamba BB. Ferrite nanoparticles: Synthesis, characterisation and applications in electronic device. Materials Science and Engineering: B. 2017;215:37-55.
8. Ghaffari A, Abazari M, Moghimi HR. Wound healing and nanotechnology: opportunities and challenges. Bioengineered Nanomaterials for Wound Healing and Infection Control: Elsevier; 2023. p. 115-174.
9. Rashidzadeh H, Tabatabaei Rezaei SJ, Adyani SM, Abazari M, Rahamooz Haghighi S, Abdollahi H, Ramazani A. Recent advances in targeting malaria with nanotechnology-based drug carriers. Pharmaceutical Development and Technology. 2021;26(8):807-823.
10. Speliotis D. Magnetic recording beyond the first 100 Years. Journal of Magnetism and Magnetic Materials. 1999;193(1-3):29-35.
11. Younas M, Nadeem M, Atif M, Grossinger R. Metal-semiconductor transition in $NiFe_2O_4$ nanoparticles due to reverse cationic distribution by impedance spectroscopy. Journal of Applied Physics. 2011;109(9).

12. Abazari M, Ghaffari A, Rashidzadeh H, Badeleh SM, Maleki Y. A Systematic Review on Classification, Identification, and Healing Process of Burn Wound Healing. The International Journal of Lower Extremity Wounds. 2020;21(1):18-30.
13. Kingery WD, Bowen HK, Uhlmann DR, Frieser R. Introduction to Ceramics. Journal of The Electrochemical Society. 1977;124(3):152C-152C.
14. Özgür Ü, Alivov Y, Morkoç H. Microwave ferrites, part 1: fundamental properties. Journal of Materials Science: Materials in Electronics. 2009;20(9):789-834.
15. Abazari M, Jamjah R, Bahri-Laleh N, Hanifpour A. Synthesis and evaluation of a new three-metallic high-performance Ziegler–Natta catalyst for ethylene polymerization: experimental and computational studies. Polym Bull. 2021;79(9):7265-7280.
16. Pang YL, Lim S, Ong HC, Chong WT. Research progress on iron oxide-based magnetic materials: Synthesis techniques and photocatalytic applications. Ceram Int. 2016;42(1):9-34.
17. Xiong K, Wang B-W, Sun Z-P, Li W, Jin C-C, Zhang S-M, et al. Frist-principles prediction of elastic, electronic, and thermodynamic properties of high entropy carbide ceramic (TiZrNbTa)C. Rare Metals. 2021;41(3):1002-1014.
18. Verma A, Goel TC, Mendiratta RG, Gupta RG. High-resistivity nickel–zinc ferrites by the citrate precursor method. Journal of Magnetism and Magnetic Materials. 1999;192(2):271-276.
19. Eltabey MM, Agami WR, Mohsen HT. Improvement of the magnetic properties for Mn–Ni–Zn ferrites by rare earth Nd3+ ion substitution. Journal of Advanced Research. 2014;5(5):601-605.
20. Ghasemi A, Hossienpour A, Morisako A, Saatchi A, Salehi M. Electromagnetic properties and microwave absorbing characteristics of doped barium hexaferrite. Journal of Magnetism and Magnetic Materials. 2006;302(2):429-435.
21. Abazari M, Jamjah R, Abdollahi H. Investigation of Optimal Condition of Ethylene Polymerization Using a New Three-Metallic High-Performance Ziegler–Natta Catalyst: Experimental Design and Polymer Characterization. Catalysis Letters. 2022;153(2):622-633.
22. K. Tyagi A, Singh Ahlawat D. Influence of pH Variation on Structural and Magnetic Properties of Ni-Zn Ferrite Nanoparticles Synthesized by Auto Combustion Method. Oriental Journal of Chemistry. 2017;33(1):296-303.
23. Abazari M, Akbari T, Hasani M, Sharifikolouei E, Raoufi M, Foroumadi A, et al. Polysaccharide-based hydrogels containing herbal extracts for wound healing applications. Carbohydr Polym. 2022;294:119808.
24. Elsayed EM, Rashad MM, Khalil HFY, Ibrahim IA, Hussein MR, El-Sabbah MMB. The effect of solution pH on the electrochemical performance of nanocrystalline metal ferrites MFe_2O_4 (M=Cu, Zn, and Ni) thin films. Applied Nanoscience. 2015;6(4):485-494.
25. Jasso-Terán RA, Cortés-Hernández DA, Sánchez-Fuentes HJ, Reyes-Rodríguez PY, León-Prado LE. Nanopartículas magnéticas de zinc y calcio para aplicaciones en hipertermia magnética. Revista Facultad de Ingeniería. 2016;25(42):89-98.
26. Paresque MCdC, Oliveira EMd, Campos MFd, Castro JAd. Análise por nta/tga/dsc das caracteristicas do revestimento de nanoparticulas de magnetita para tratamento de hipertermia magnética. ABM Proceedings; 2019/02: Editora Blucher; 2019.
27. Lafta SH. Effect of pH on Structural, Magnetic and FMR Properties of Hydrothermally Prepared Nano Ni Ferrite. Open Chemistry. 2017;15(1):53-60.
28. Jadhav Santosh S, Shirsath Sagar E, G. Toksha B, J. Shukla S, M. Jadhav K. Effect of Cation Proportion on the Structural and Magnetic Properties of Ni-Zn Ferrites Nano-Size Particles Prepared By Co-Precipitation Technique. ChJCP. 2008;21(4):381-386.
29. Huq MF, Saha DK, Ahmed R, Mahmood ZH. Ni-Cu-Zn Ferrite Research: A Brief Review. Journal of Scientific Research. 2013;5(2):215-234.
30. Shahbahrami B, Rabiee SM, Shidpoor R. Effect of pH Value on Synthesis and Properties of Zinc Cobalt Ferrite Nano Powders Prepared via Co-Precipitation Method. Research Square Platform LLC; 2020.
31. Hasan S, Azhdar B. Synthesis of Nickel-Zinc Ferrite Nanoparticles by the Sol-Gel Auto-Combustion Method: Study of Crystal Structural, Cation Distribution, and Magnetic Properties. Advances in Condensed Matter Physics. 2022;2022:1-14.
32. Abazari M, Badeleh SM, Khaleghi F, Saeedi M, Haghi F. Fabrication of silver nanoparticles-deposited fabrics as a potential candidate for the development of reusable facemasks and evaluation of their performance. Sci Rep. 2023;13(1).
33. Boyd I, Chrisey DB. Pulsed laser deposition of thin films. Handbook of Laser Technology and Applications: IOP Publishing Ltd.
34. Christen HM, Eres G. Recent advances in pulsed-laser deposition of complex oxides. J Phys: Condens Matter. 2008;20(26):264005.
35. Junaid M, Khan MA, Abubshait SA, Akhtar MN, Kattan NA, Laref A, Asif Javed HM. Structural, spectral, dielectric and magnetic properties of indium substituted copper spinel ferrites synthesized via sol gel technique. Ceram Int. 2020;46(17):27410-27418.
36. Mohapatra PP, Pittala S, Dobbidi P. Temperature dependent broadband dielectric, magnetic and electrical studies on $Li_{1-x}Mg_{2x}Fe_{5-x}O_8$ for microwave devices. Journal of Materials Research and Technology. 2020;9(3):2992-3004.
37. Powar RR, Phadtare VD, Parale VG, Pathak S, Sanadi KR, Park H-H, et al. Effect of zinc substitution on magnesium ferrite nanoparticles: Structural, electrical, magnetic, and gas-sensing properties. Materials Science and Engineering: B. 2020;262:114776.
38. Jose R, J R, Jothi NSN. The synthesis and characterisation of curcumin loaded $Ag_{(1-X)}Ni_xFe_2O_4$ for drug delivery. Materials Technology. 2020;36(6):339-346.
39. Chen H. Applications of Lignocellulose Biotechnology in the Chemical Industry. Biotechnology of Lignocellulose: Springer Netherlands; 2014. p. 247-300.
40. Ahmed MM, Ameen MSM, Abazari M, Badeleh SM, Rostamizadeh K, Mohammed SS. Chitosan-decorated and tripolyphosphate-crosslinked pH-sensitive niosomal nanogels for Controlled release of fluoropyrimidine 5-fluorouracil. Biomedicine & Pharmacotherapy. 2023;164:114943.
41. Hong S-J, Mun H-J, Kim B-J, Kim Y-S. Characterization of Nickel Oxide Nanoparticles Synthesized under Low Temperature. Micromachines. 2021;12(10):1168.
42. Sharma AK, Desnavi S, Dixit C, Varshney U, Sharma A. Extraction of Nickel Nanoparticles from Electroplating Waste and Their Application in Production of Bio-diesel from Biowaste. International Journal of Chemical Engineering and Applications. 2015;6(3):156-159.